Phosphoinositide-mediated ring anchoring resists perpendicular forces to promote medial cytokinesis

Chloe E. Snider,* Alaina H. Willet,* Jun-Song Chen, Göker Arpağ, Marija Zanic, and Kathleen L. Gould

Department of Cell and Developmental Biology, Vanderbilt University, Nashville, TN

Many eukaryotic cells divide by assembling and constricting an actin- and myosin-based contractile ring (CR) that is physically linked to the plasma membrane (PM). In this study, we report that *Schizosaccharomyces pombe* cells lacking *efr3*, which encodes a conserved PM scaffold for the phosphatidylinositol-4 kinase Stt4, build CRs that can slide away from the cell middle during anaphase in a myosin V–dependent manner. The Efr3-dependent CR-anchoring mechanism is distinct from previously reported pathways dependent on the Fes/CIP4 homology Bin-Amphiphysin-Rvs167 (F-BAR) protein Cdc15 and paxillin Pxl1. In *efr3Δ*, the concentrations of several membrane-binding proteins were reduced in the CR and/or on the PM. Our results suggest that proper PM lipid composition is important to stabilize the central position of the CR and resist myosin V–based forces to promote the fidelity of cell division.

Introduction

To divide, many eukaryotes assemble and constrict an actin- and myosin-based contractile ring (CR; Cheffings et al., 2016) that is anchored to the plasma membrane (PM; Gould, 2016). Despite decades of work on how the division plane is selected and the CR assembles (Pollard and Wu, 2010; Bohnert and Gould, 2011; Goyal et al., 2011; Lee et al., 2012; Rincon and Paoletti, 2016), mechanisms of CR–PM anchoring remain incompletely understood.

One factor implicated in CR–PM attachment is PM lipid composition. Phosphatidylinositol (PI)-4,5-bisphosphate ($PI(4,5)P_2$) and PI5 kinases are enriched at the cleavage furrow of mammalian cells, and when $PI(4,5)P_2$ is depleted, cortical actin separates from the PM (Emoto et al., 2005; Field et al., 2005). CR components such as RhoA, anillin, and MgcRacGAP bind $PI(4,5)P_2$ (Cauvin and Echard, 2015); therefore, they may mislocalize when $PI(4,5)P_2$ levels are reduced. A decrease in cortically bound anillin may be particularly detrimental to CR–PM attachment because anillin binds components of the CR and $PI(4,5)P_2$ (Piekny and Glotzer, 2008; D'Avino, 2009; Sun et al., 2015). In human and *Drosophila melanogaster* cells, anillin loss causes cleavage furrow oscillations (Kechad et al., 2012). However, the exact combination of molecules involved in CR detachment when $PI(4,5)P_2$ is depleted remains to be determined.

Schizosaccharomyces pombe build a medial CR early in mitosis (Marks and Hyams, 1985; Kitayama et al., 1997). How the CR remains anchored until constriction is not yet clear, although several players have been implicated. One is the Fes/CIP4 homology Bin-Amphiphysin-RVS (F-BAR) protein Cdc15: when *cdc15* expression is repressed or Cdc15 oligomerization is disrupted, the CR can slide along the PM and disassemble (Arasada and Pollard, 2014; McDonald et al., 2015). Paxillin Pxl1 also plays a role in CR anchoring and integrity, indicated by CR sliding and splitting during anaphase in *pxl1Δ* (Ge and Balasubramanian, 2008; Cortés et al., 2015). Another factor is the cell wall: loss of β(1,3)glucan (Muñoz et al., 2013) or loss of the integral membrane protein Sbg1 (Davidson et al., 2016; Sethi et al., 2016) result in CR sliding and instability, suggesting that cell wall–PM linkage is important for CR maintenance. Finally, the microtubule post-anaphase array ensures a medial CR during a cytokinesis arrest (Pardo and Nurse, 2003). In each of these situations, CR sliding is observed in only a fraction of cells (Pardo and Nurse, 2003; Arasada and Pollard, 2014; Cortés et al., 2015; McDonald et al., 2015), indicating that multiple mechanisms contribute to CR anchoring. Consistent with this, combined repression of *pxl1* with a hypomorphic *cdc15* allele results in exacerbated CR sliding (Cortés et al., 2015).

In this study, we define a distinct mechanism that anchors CRs during anaphase, explaining why cells lacking *S. pombe efr3* divide asymmetrically (Chen et al., 2015). In *Saccharomyces cerevisiae*, Efr3 and its partner Ypp1 form a platform at the PM for Stt4, a PI4 kinase, which regulates phosphoinositide (PIP) composition and supports endocytosis (Baird et al., 2008). Similarly, human homologues of Efr3 and Ypp1 (EFR3A/B and TTC7) scaffold a PI4 kinase type-IIIα at the PM (Nakatsu et al., 2012).

We find that *S. pombe* lacking properly positioned Stt4 have altered PM PIPs. These cells form CRs in the cell middle that can then slide toward one end in a directed manner. CR

*C.E. Snider and A.H. Willet contributed equally to this paper.

Correspondence to Kathleen L. Gould: kathy.gould@vanderbilt.edu

Abbreviations used: CR, contractile ring; F-BAR, Fes/CIP4 homology Bin-Amphiphysin-RVS; mNG, mNeonGreen; MSD, mean squared displacement; PH, Pleckstrin homology; PI, phosphatidylinositol; $PI(4,5)P_2$, PI-4,5-bisphosphate; PI4P, PI-4-phosphate; PIP, phosphoinositide; PM, plasma membrane; ROI, region of interest; YE, yeast extract.

The Rockefeller University Press
J. Cell Biol. Vol. 216 No. 10 3041–3050
https://doi.org/10.1083/jcb.201705070

sliding in *efr3Δ* requires the type V myosin Myo51, indicating for the first time that the CR is subject to perpendicular forces in addition to being under constrictive tension (Proctor et al., 2012) and that these forces can dislodge the CR from the cell center. Thus, PM PIP composition contributes to CR anchoring, promoting proper septum positioning and ensuring accurate genome segregation.

Results and discussion

We previously observed that a high percentage of *efr3Δ* divide asymmetrically (Fig. 1 A), sometimes resulting in the cutting of chromosomes by off-center septa (Chen et al., 2015). To determine whether this is caused by altered PM PIP composition, we first determined whether Efr3 colocalizes with Stt4 and Ypp1 in *S. pombe* by analyzing the localization of three distinct pairs of these proteins tagged with mCherry and mNeonGreen (mNG) or GFP. Each pair colocalized on the PM in a punctate pattern (Fig. 1 B), resembling the PI kinase patch localization of the *S. cerevisiae* Stt4 complex (Baird et al., 2008). The PM enrichment of *S. pombe* Stt4 and Ypp1, but not their levels, depended on Efr3 (Fig. 1 C). Efr3 coimmunoprecipitated with Ypp1 (Fig. S1 A), and both Ypp1 and Stt4 were identified in an Efr3-TAP by liquid chromatography–tandem mass spectrometry analysis (Fig. S1 B and Table S2), indicating that these proteins associate in *S. pombe*. To further study the influence of Stt4 on septa positioning, we attempted to construct *stt4Δ* and *ypp1Δ* but found that these genes are essential (Fig. S1, C and D). However, endogenously tagged GFP-*stt4* displayed off-center septa, indicating that although GFP-Stt4 localizes correctly to the PM, it is likely to be a hypomorphic allele (Fig. 1, A and B). These data establish that proteins of the Stt4 complex are important for medial division.

Stt4 phosphorylates PM PI to produce PI-4-phosphate (PI4P), which can be further modified to $PI(4,5)P_2$. Therefore, disruption of PI4 kinases results in a reduction of both PI4P and $PI(4,5)P_2$ (Audhya and Emr, 2002; Baird et al., 2008; Nakatsu et al., 2012). The $PI(4,5)P_2$ sensor GFP-2×PH(PLCδ) (Stefan et al., 2002) was reduced at the cell cortex and the division site in *efr3Δ* compared with WT (Fig. 1 D), indicating that PIP PM abundance is reduced in *efr3Δ*. In accordance with this, overexpression of GFP-2×PH(PLCδ), expected to sequester $PI(4,5)P_2$, resulted in off-center septa (Fig. 1 E).

We next addressed how off-center septa arise in *efr3Δ*. Because septum position is dictated by CR position (Marks and Hyams, 1985; Marks et al., 1986), we reasoned that either the CR forms off-center or it slides from its original medial position. To distinguish between these possibilities, we imaged WT and *efr3Δ* expressing CR (Rlc1-GFP) and spindle pole body (Sid4-GFP) markers. In WT, the CR formed in the cell center and maintained this position during cytokinesis (Fig. 2 A). In *efr3Δ*, the CR formed in the cell center but slid from its original position while remaining perpendicular to the cell's long axis (Fig. 2, A–C). Temporal progression through cytokinesis was unchanged in *efr3Δ* compared with WT (Fig. S2, A and B). CR sliding occurred during anaphase B, after the CR formed in early mitosis, but stopped before or coincidently with CR constriction (Fig. 2, A and D). This indicates that the CR cannot slide in *efr3Δ* once septation begins, likely because septum formation locks the CR in position (Muñoz et al., 2013; for review, see Willet et al., 2015).

CR sliding, indicative of a CR anchoring defect, was observed when oligomerization of Cdc15's F-BAR domain was prevented or when *cdc15* expression was repressed (Arasada and Pollard, 2014; McDonald et al., 2015). To determine whether Cdc15-mediated CR anchoring involves Efr3, we compared CR sliding events in *efr3Δ* and *cdc15–core 4A*, a mutant that specifically impairs membrane binding (McDonald et al., 2015). Alone, *cdc15–core 4A* displayed CR sliding. When combined with *efr3Δ,* the frequency of CR sliding events was increased compared with each single mutant (Fig. 2, A and B). Also, CRs slid farther in the double mutant, indicated by the lower mean ratio of short to long cells at septation (Fig. 2 C), ultimately leading to growth defects (Fig. 2 E). Therefore, Cdc15- and Efr3-mediated CR anchoring are independent mechanisms that maintain central CR positioning. Mutants of *pxl1* also display CR sliding (Cortés et al., 2015); however, *pxl1Δ efr3Δ* was inviable (Fig. S2 D), suggesting that Pxl1 contributes to CR anchoring independently of Efr3. Because *efr3Δ* does not change the kinetics of cytokinesis (Fig. S2, A and B) as defects in the β-glucan enzymes Bgs1 and Bgs4 do (Muñoz et al., 2013; Davidson et al., 2016; Sethi et al., 2016), Efr3-dependent anchoring appears to be an independent mechanism from cell wall anchoring as well.

Because *efr3Δ* has reduced levels of PM $PI(4,5)P_2$, we hypothesized that the cortical enrichment of proteins with membrane-binding domains (F-BAR, Pleckstrin homology [PH], Phox homology domain [PX], or C2) would be diminished in *efr3Δ* compared with WT. Consistent with Cdc15 acting independently of Efr3 and interacting with a wide range of anionic phospholipids (McDonald et al., 2015), we found no difference in Cdc15 CR intensity (Fig. 3, A and B). The localizations of many other membrane-binding proteins, such as Pob1 (Fig. S2 E), were also unaltered in *efr3Δ* (Fig. 3 A), suggesting that they do not rely upon PI4P or $PI(4,5)P_2$. However, we identified three PH domain–containing proteins with reduced PM localization in *efr3Δ* compared with WT. The RhoGEF Rgf1 and Cdc42 GEF Scd1 were reduced at the division site without any reduction in total protein levels (Fig. 3, C and D). Opy1, encoded by the ORF SPCPB16A4.02c, is normally enriched at the PM but was diffusely localized in *efr3Δ* (Fig. 3 E). Opy1 contains two PH domains, and the *S. cerevisiae* orthologue Opy1 is implicated in sensing PI4P at the PM and inhibiting the PI5 kinase Mss4 (Its3 in *S. pombe*; Ling et al., 2012). Thus, it may be a collective reduction of several proteins at the cortex that compromises CR–PM attachment in *efr3Δ*.

Off-center septa in *S. pombe* are observed when CRs slide and also when they assemble off center. Mid1 and Pom1 dictate CR positioning (Rincon and Paoletti, 2016); cells lacking either divide asymmetrically because of misplaced CRs (Chang et al., 1996; Sohrmann et al., 1996; Bähler and Pringle, 1998; Bähler et al., 1998a). In *mid1Δ*, CRs assemble at random positions and angles along the cortex but eventually coalesce into an orthogonal CR (Huang et al., 2008); although if CRs form within the curved cell pole of *mid1–18,* they can slide toward the tip, decreasing in diameter (Mishra et al., 2012). To test whether the Mid1 and Pom1 cues are influenced by PM composition, given that both proteins bind membrane PIPs (Celton-Morizur et al., 2004; Hachet et al., 2011), we combined *mid1Δ* or *pom1Δ* with *efr3Δ* and analyzed CR dynamics. We scored whether CRs formed off-center and whether fully formed CRs slid during anaphase. In our experiments, *mid1Δ* rarely formed CRs at the extreme cell tip that slid. As previously observed, *mid1Δ* and

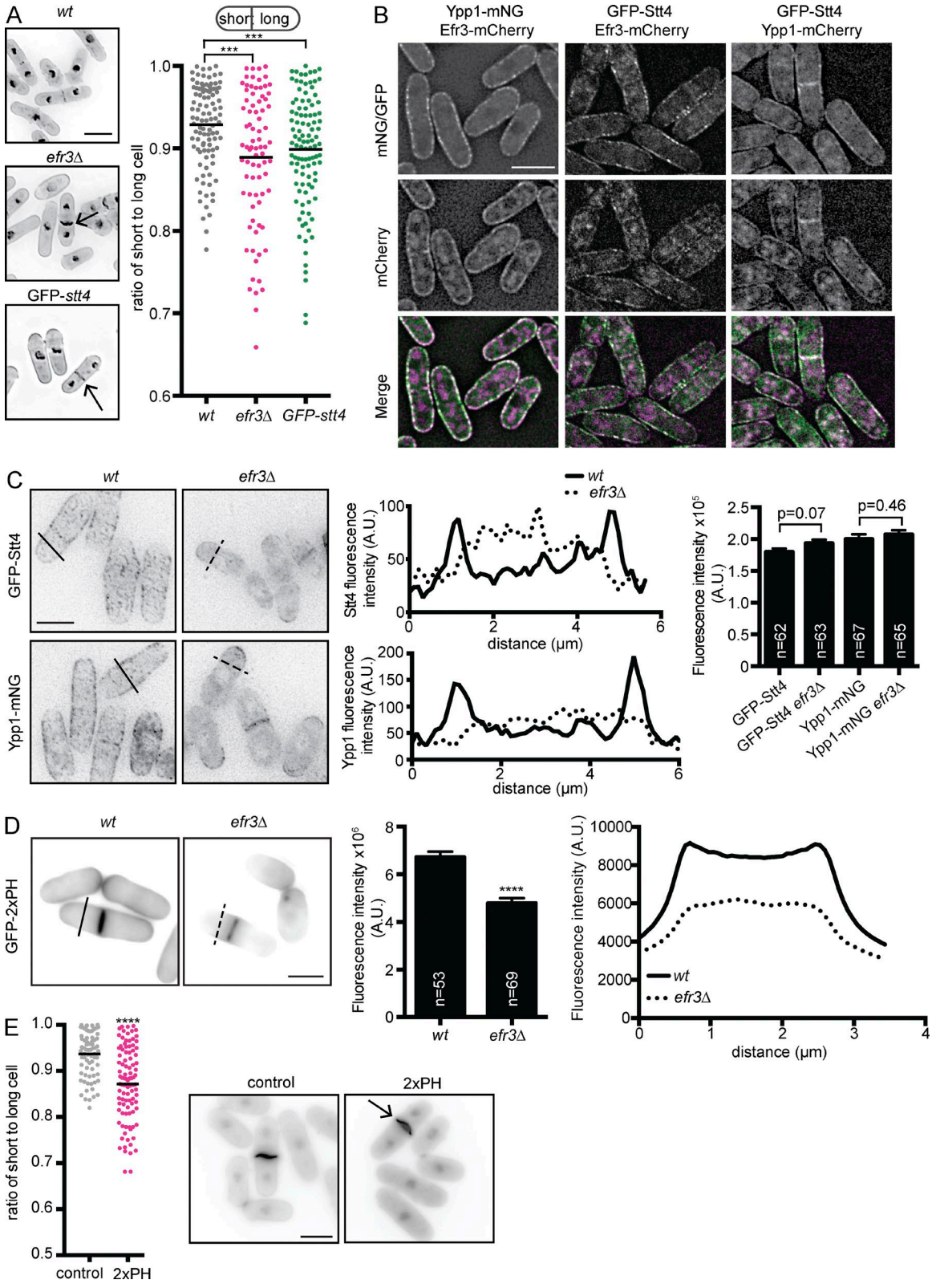

Figure 1. ***efr3Δ* display off-center septa.** (A, left) Representative images of indicated strains stained for cell walls and nuclei. Arrows indicate off-center septa. (A, right) Schematic of centered and off-centered septa classification and quantification. Individual points represent the ratio of the length of the short to long daughter cells at septation, and black bars denote means. (B) Live-cell images of the indicated strains are of a single medial z slice. (C, left) GFP-Stt4 or Ypp1-mNG in either WT or *efr3Δ*. Images are z projections and are not identically scaled. (C, middle) Line scans of the fluorescence intensity of the solid (WT) and dotted (*efr3Δ*) black lines shown in left panels. (C, right) Whole-cell fluorescence intensity of the indicated strains. (D, left) Representative images of GFP-2xPH(PLCδ) localization in either WT or *efr3Δ*. (D, middle) Quantification of the fluorescence intensity at the division septum. (D, right) Line scans

pom1Δ form off-center CRs, but we did not detect a significant number of subsequent sliding events (Chang et al., 1996; Sohrmann et al., 1996; Bähler and Pringle, 1998). Consistent with our finding that initial CR placement is not altered in *efr3Δ*, the localizations of PM-binding proteins Mid1 and Pom1 were not influenced by deletion of *efr3* (Fig. 3 A). In combination with *efr3Δ*, *mid1Δ* and *pom1Δ* CRs formed off-center and slid during anaphase, resulting in septa that were farther off-center than single mutants (Fig. 4, A–C). These combinations also led to significant growth defects (Fig. 4 D), most likely a result of chromosomes being cut by off-center septation.

We next considered whether CR sliding events in *efr3Δ* are enabled by diminishing cell circumference from the cell middle toward one end, similar to CRs in spheroplasts, which move along the cortex while constricting (Mishra et al., 2013). This seemed unlikely, however, because *efr3Δ* has normal morphology (Chen et al., 2015) and CRs slide only 1–2 µm (Fig. 2 A), not approaching the region of curvature at the hemispherical cell ends (Atilgan et al., 2015). Also, *pos5Δ*, which is tapered at one cell end (Hayles et al., 2013), does not have off-center septa, indicating that a CR does not automatically slide toward a tapered end (Fig. S2 C). The CR width, as a proxy of cell diameter, also does not decrease during a sliding event in *efr3Δ*, which would be expected if the circumference of the cell changed (Δ width = 0.045 µm ± 0.039 µm [SEM; $n = 19$]). Furthermore, in *pos5Δ efr3Δ*, there was no worsening of the off-center septa phenotype compared with *efr3Δ* (Fig. S2 C), and sliding CRs had no bias toward the tapered end of the cell (54% to the tapered end vs. 46% to the nontapered end), similar to *efr3Δ*, where the CR is equally likely to slide to the old or new end of the cell (48% to the old end vs. 52% to the new end). We conclude that CR sliding events in *efr3Δ* are not dictated by cell geometry.

Because CR sliding in spheroplasts and *cdc15*-defective cells depends on the type II myosins Myo2 and Myp2, respectively (Mishra et al., 2013; Arasada and Pollard, 2014), we tested whether myosin-generated force is required for CR sliding in *efr3Δ*. Neither Myp2, the type I myosin Myo1, nor the type V myosin Myo52 were necessary for CR sliding in *efr3Δ* (Fig. 5 A). To test whether CR sliding depends on Myo2, we attempted to combine *efr3Δ* with the temperature-sensitive *myo2-E1* allele (Balasubramanian et al., 1998), but these alleles were synthetically lethal (Fig. S3 A). Instead, we used a *myo2-E1* GFP-*stt4* combination. GFP-*stt4* (GFP-*stt4* is hypomorphic) and *myo2-E1* each had off-center septa at 32°C, and the combination resulted in more cells with off-center septa that were even farther away from center (Fig. S3 B). Live-cell imaging revealed that GFP-*stt4* CRs slid during anaphase, whereas *myo2-E1* CRs formed off-center but did not slide (Fig. S3 C). GFP-*stt4 myo2-E1* formed CRs off-center that then also slid along the cortex (Fig. S3 C). Thus, CR sliding in *efr3Δ* does not depend on Myo2.

In contrast, deletion of the type V myosin Myo51 eliminated the *efr3Δ* off-center septa phenotype (Fig. 5 A). CR sliding events no longer occurred in *myo51Δ efr3Δ* (Fig. 5, B and C), and the mean ratio of short to long cells was significantly higher than in *efr3Δ* (Fig. 5 A). As expected given that Stt4 binds Efr3, the GFP-*stt4* off-center septa phenotype is also Myo51 dependent (Fig. S3 B). None of the myosins were necessary for CR sliding in *cdc15–core 4A* or *pxl1Δ* mutants (Fig. S3, D and E), consistent with the genetic evidence that Cdc15-, Pxl1-, and Efr3-dependent CR sliding events occur through independent mechanisms (Figs. 2 E and S2 D; Cortés et al., 2015). Indeed, CR sliding in *cdc15* and *pxl1Δ* mutants as well as in β-glucan synthase mutations may occur because of structural instability of the CR rather than a directed movement of the CR along the cortex (Balasubramanian et al., 1998; Arai and Mabuchi, 2002; Wachtler et al., 2006; Ge and Balasubramanian, 2008; Hachet and Simanis, 2008; Roberts-Galbraith et al., 2009; Laporte et al., 2011; Muñoz et al., 2013; Arasada and Pollard, 2014; McDonald et al., 2015; Davidson et al., 2016; Sethi et al., 2016).

Myo51 contains an N-terminal motor head domain and a C-terminal tail domain necessary for CR localization (Wang et al., 2014). By testing Myo51 N- and C-terminal truncations in *efr3Δ*, we found that both the N-terminal head and C-terminal tail of Myo51 are necessary for CR sliding (Fig. S3 F), suggesting that Myo51 tail binding to CR components and the ability to walk along actin filaments (Wang et al., 2014) are both required to move the CR.

The necessity of Myo51 force generation for CR movements in *efr3Δ* provides strong evidence for the existence of forces on the CR perpendicular to the cell axis. Such forces could be involved in the splitting of CRs observed in some mutants, e.g., *pxl1Δ* (Ge and Balasubramanian, 2008) and *sbg1–3* (Sethi et al., 2016). We hypothesize that perpendicular forces are balanced in a WT cell and/or that CR–PM attachments are sufficient to resist these forces so that the CR remains in its central position. In *efr3Δ*, force imbalances may arise that cannot be stabilized, resulting in Myo51-dependent CR sliding along the cell axis. In support of this hypothesis, mean squared displacement (MSD) analysis of sliding *efr3Δ* CRs shows a statistically significant drift velocity term, suggesting directed transport of the CR (Fig. S3 G; v = 1.35 nm/s; 95% confidence interval, 1.32–1.37 nm/s). No such transport term was measured for WT rings, which exhibit minimal changes in position over the imaging period (Fig. S3 G; also see the MSD analysis section of Materials and methods). A possible explanation for this behavior is that Myo51 in the CR associates with longitudinal actin cables as well as F-actin within the CR, pulling the CR along cables when PM anchoring is weakened. In support of this, Myo51 has been shown to play a role in the medial accumulation of actin cables during cytokinesis (Huang et al., 2012), and actin cables can be seen in proximity to sliding CRs in *efr3Δ* (Fig. 5 D).

Altogether, our data reveal a novel CR anchoring mechanism that depends on a conserved PM-localized PI4 kinase complex (Fig. 5 E). An ensemble of proteins sensitive to correct PM PIP composition synergize with Cdc15-, Pxl1-, and cell wall–dependent anchoring to promote stable CR placement and faithful segregation of the genetic material during cell division. A cytokinetic function for Stt4 or its human orthologues has not been previously reported, but a related PI4 kinase is important for *Drosophila* cytokinesis (Brill et al., 2000; Eggert et al., 2004). Given the large number of lipid-binding proteins at the cell division site of many eukaryotes, PI4 kinases are likely to be a generally important factor for CR–PM adhesion.

of the fluorescence intensity of the solid (WT) and dotted (*efr3Δ*) black lines. Data in graphs are from three biological replicates. (E) Representative images (right) and quantification (left) of cells stained for cell walls and nuclei. The arrow indicates an off-center septum. Error bars represent SEM. (A, C, D, and E) ***, $P \leq 0.001$; ****, $P \leq 0.0001$; one-way ANOVA (A) or Student's *t* test (C, D, and E). Bars, 5 µm.

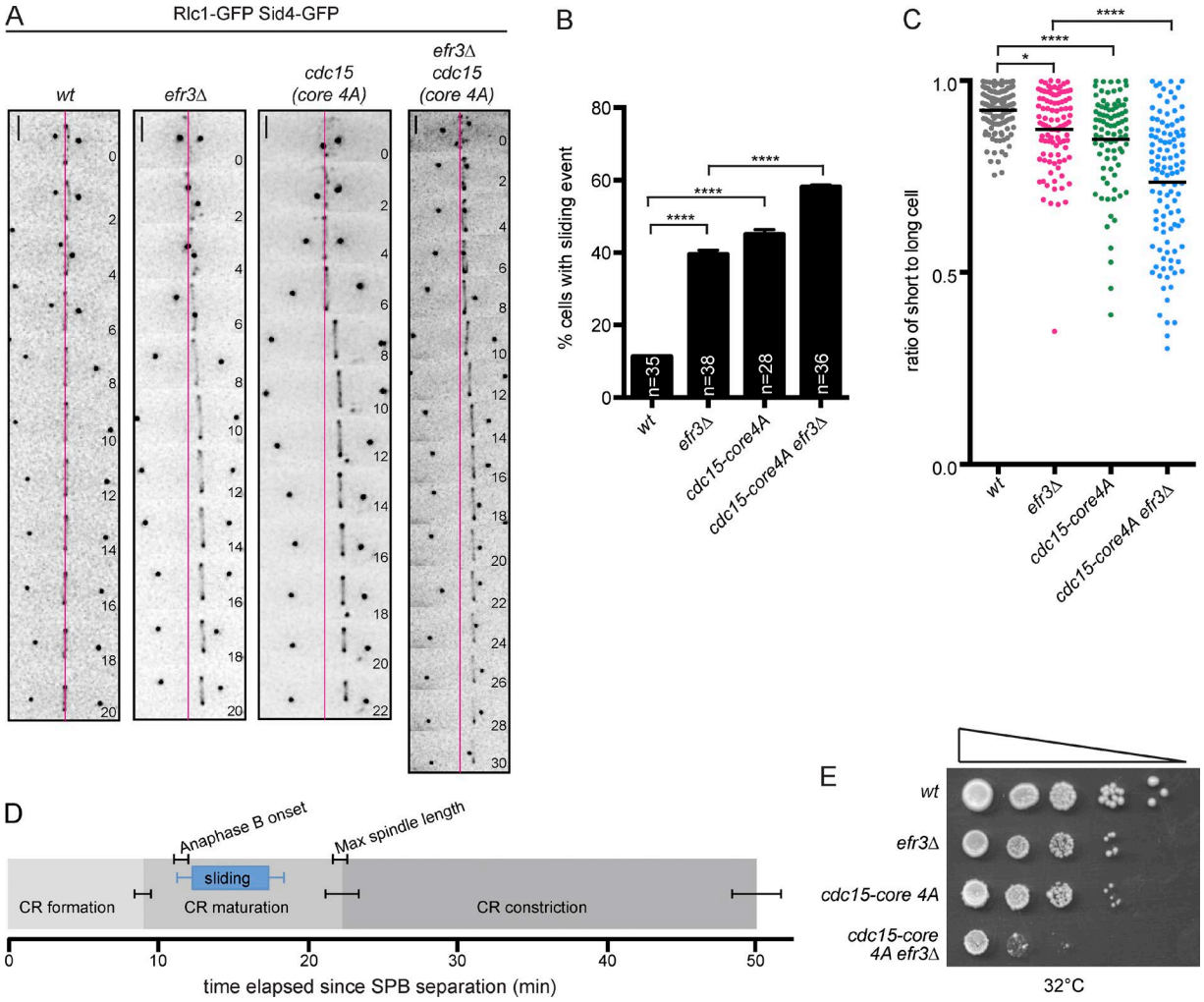

Figure 2. **CRs slide in *efr3Δ*.** (A) Live-cell imaging of indicated strains expressing Rlc1-GFP and Sid4-GFP. Magenta lines mark the cell center. Elapsed time is provided in minutes. Bars, 2 µm. (B) Quantification of the frequency of CR sliding events in the indicated strains determined as in A. (C) Quantification of off-center septa. Individual points represent the ratio of the length of the short to long daughter cells at septation, and black bars denote means. Error bars represent SEM. *, $P \leq 0.05$; ****, $P \leq 0.0001$; one-way ANOVA. (D) Mean timing of mitotic events in *efr3Δ* cells. SPB, spindle pole body. (E) Growth assay of serial 10-fold dilutions of the indicated strains at 32°C on YE media.

Materials and methods

Yeast methods

S. pombe strains (Table S1) were grown in yeast extract (YE). *efr3*$^+$, *ypp1*$^+$, *opy1*$^+$, *scd1*$^+$, and *rgf1*$^+$ were tagged at the 3′ end of their ORFs with TAP:kan^R, Flag$_3$:kan^R, HA$_3$:hyg^R, mCherry:kan^R, mNG:kan^R, or mNG:hyg^R using pFA6 cassettes as previously described (Wach et al., 1994; Bähler et al., 1998b). A lithium acetate method (Keeney and Boeke, 1994) was used in *S. pombe* tagging transformations, and integration of tags was verified using whole-cell PCR and/or microscopy. Introduction of tagged loci into other genetic backgrounds was accomplished using standard *S. pombe* mating, sporulation, and tetrad dissection techniques. Fusion proteins were expressed from their native promoters at their normal chromosomal loci unless otherwise indicated. Strains producing *myo51* truncations were obtained from Dr. J.-Q. Wu (Wang et al., 2014).

For growth assays, cells were grown to log phase at 25°C in YE, 10 million cells were resuspended in 1 ml of water, and 10-fold serial dilutions were made. 2.5 µl of each dilution was spotted on YE plates, and the plates were incubated at the indicated temperatures.

Stt4 was N-terminally tagged with GFP at the endogenous locus using a Cre–loxP method as described previously (Werler et al., 2003). A cassette with the sequence that encodes GFP, the *sup3–5* selection marker, and a temporary promoter (*nmt1*) were integrated at the 5′ end of the *stt4* ORF. Next, the selection marker and temporary promoter were removed with Cre recombinase, resulting in the insertion of sequences encoding GFP at the 5′ end of *stt4* under the normal promoter.

To express GFP-2×PH(PLCδ) in cells, the medium-strength *cdc2* promoter (Meddins et al., 1993) was PCR amplified from *S. pombe* genomic DNA, and GFP-2×PH(PLCδ) was PCR amplified from plasmid pRS426 (Stefan et al., 2002). The two fragments were cloned into *S. pombe* integration vector pJK148 using Gibson assembly. This construct was linearized and inserted into the *S. pombe leu1* locus by a lithium acetate method (Keeney and Boeke, 1994).

To overexpress GFP-2×PH(PLCδ), sequences encoding it were PCR amplified from plasmid pRS426 and cloned into pREP81 (Basi et al., 1993). This construct was introduced into cells by sorbitol transformation. Cells were fixed in 70% ethanol after induction of expression for 24 h at 32°C.

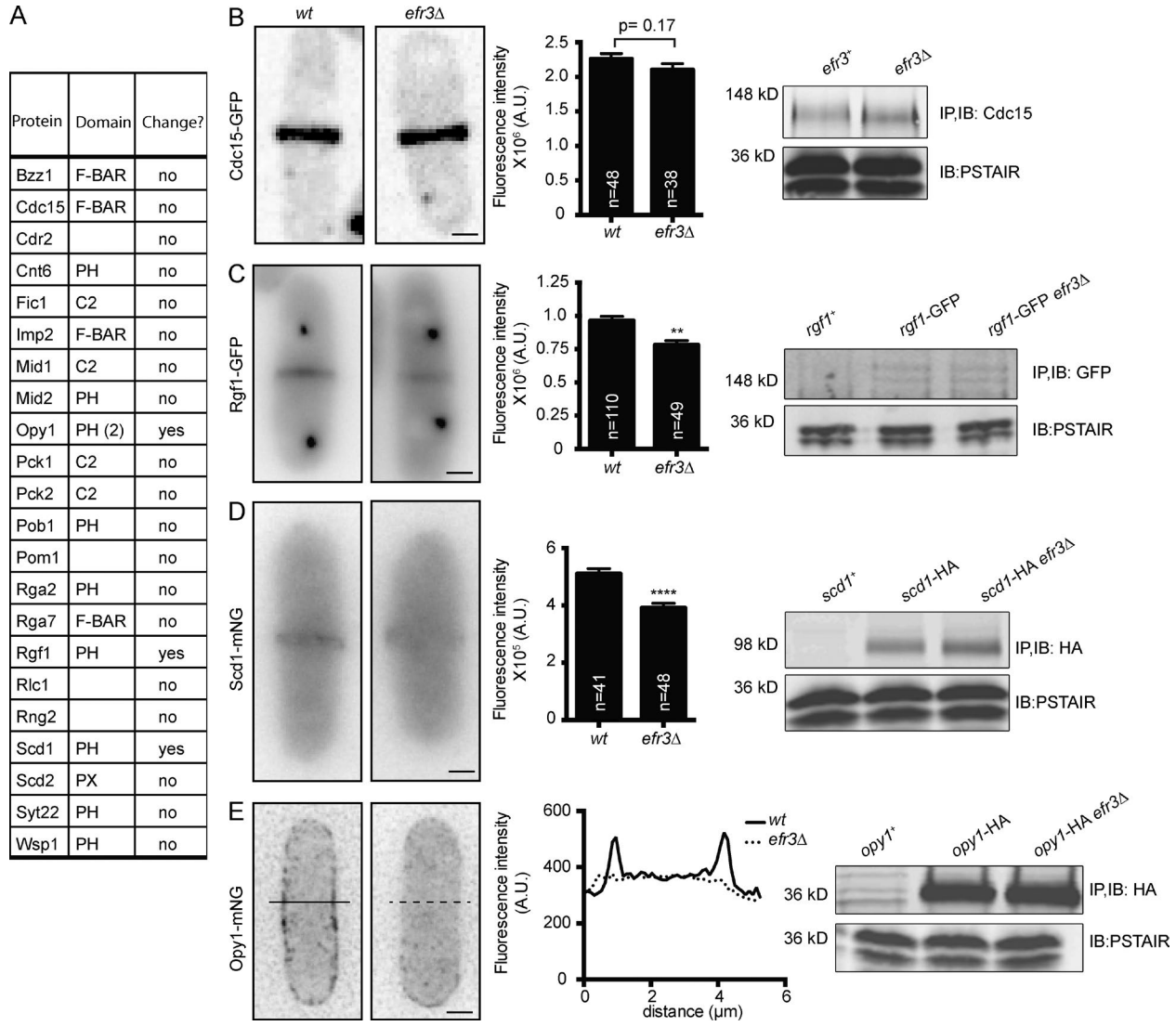

Protein	Domain	Change?
Bzz1	F-BAR	no
Cdc15	F-BAR	no
Cdr2		no
Cnt6	PH	no
Fic1	C2	no
Imp2	F-BAR	no
Mid1	C2	no
Mid2	PH	no
Opy1	PH (2)	yes
Pck1	C2	no
Pck2	C2	no
Pob1	PH	no
Pom1		no
Rga2	PH	no
Rga7	F-BAR	no
Rgf1	PH	yes
Rlc1		no
Rng2		no
Scd1	PH	yes
Scd2	PX	no
Syt22	PH	no
Wsp1	PH	no

Figure 3. **Localization of membrane-binding proteins in *efr3Δ*.** (A) List of proteins tagged with GFP or mNG and screened for differences in protein localization in *efr3Δ* compared with WT. Fluorescence intensity at the division site was measured, and statistically significant differences are noted. (B–E, left) Live-cell imaging of Cdc15-GFP (B), Rgf1-GFP Sid4-GFP (C), Scd1-mNG (D), or Opy1-mNG (E) in either WT or *efr3Δ*. (B–D, middle) Quantification of fluorescence intensity at the cell division site. (E, middle) Line scan of fluorescence intensity. (B–E, right) Western blots of protein levels in WT and *efr3Δ*. Anti-PSTAIR was used to detect Cdc2, which served as a loading control. Measurements in B–D represent three biological replicates. Error bars represent SEM. **, $P \leq 0.01$; ****, $P \leq 0.0001$; Student's *t* test. Bars, 2 µm. IB, immunoblot; IP, immunoprecipitation.

Microscopy

Live-cell images of *S. pombe* cells were acquired using a personal DeltaVision microscope system (Applied Precision Ltd.) that includes an IX71 microscope (Olympus), 60× 1.42 NA Plan Apochromat and 100× 1.40 NA U-Plan S-Apochromat objectives, a Coolsnap HQ2 camera (Photometrics), and SoftWoRx imaging software (Applied Precision Ltd.). Images were acquired at 25–29°C, and cells were imaged in YE media. Images in figures are either single slices or maximum-intensity projections of z sections spaced at 0.2–0.5 µm. Images used for quantification were not deconvolved. Other images not used for fluorescence quantification were deconvolved with 10 iterations. Time-lapse imaging was performed on cells in log phase on a YE agar pad at 32–36°C with the exception of *LifeAct-mCherry cdc25-22 efr3Δ*, where cells were shifted to 36°C for 4 h and then imaged at 25°C.

Intensity measurements were made with ImageJ software (National Institutes of Health). For all intensity measurements, the background was subtracted by creating a region of interest (ROI) in the same image where there were no cells (Waters, 2009). The raw intensity of the background was divided by the area of the background, which was multiplied by the area of the ROI. This number was subtracted from the raw integrated intensity of that ROI (Waters, 2009). For CR intensity quantification, an ROI was drawn around the CR and measured for raw integrated density.

All cells were grown to log phase at 32°C before fixation. For nuclei and cell wall imaging, cells were fixed in 70% ethanol for 30 min before DAPI and methyl blue staining.

For quantification of ring sliding, a line was drawn through the fully formed CR marked by Rlc1-GFP using ImageJ software. Any movement of the CR away from the original line placement during the entire length of imaging was scored as a ring sliding event. For ring sliding distances, fixed cells stained for nuclei and cell walls were imaged. The coordinates of the cell tips and septum were logged. Lengths of the shorter and longer cell were calculated from these coordinates and reported as a ratio.

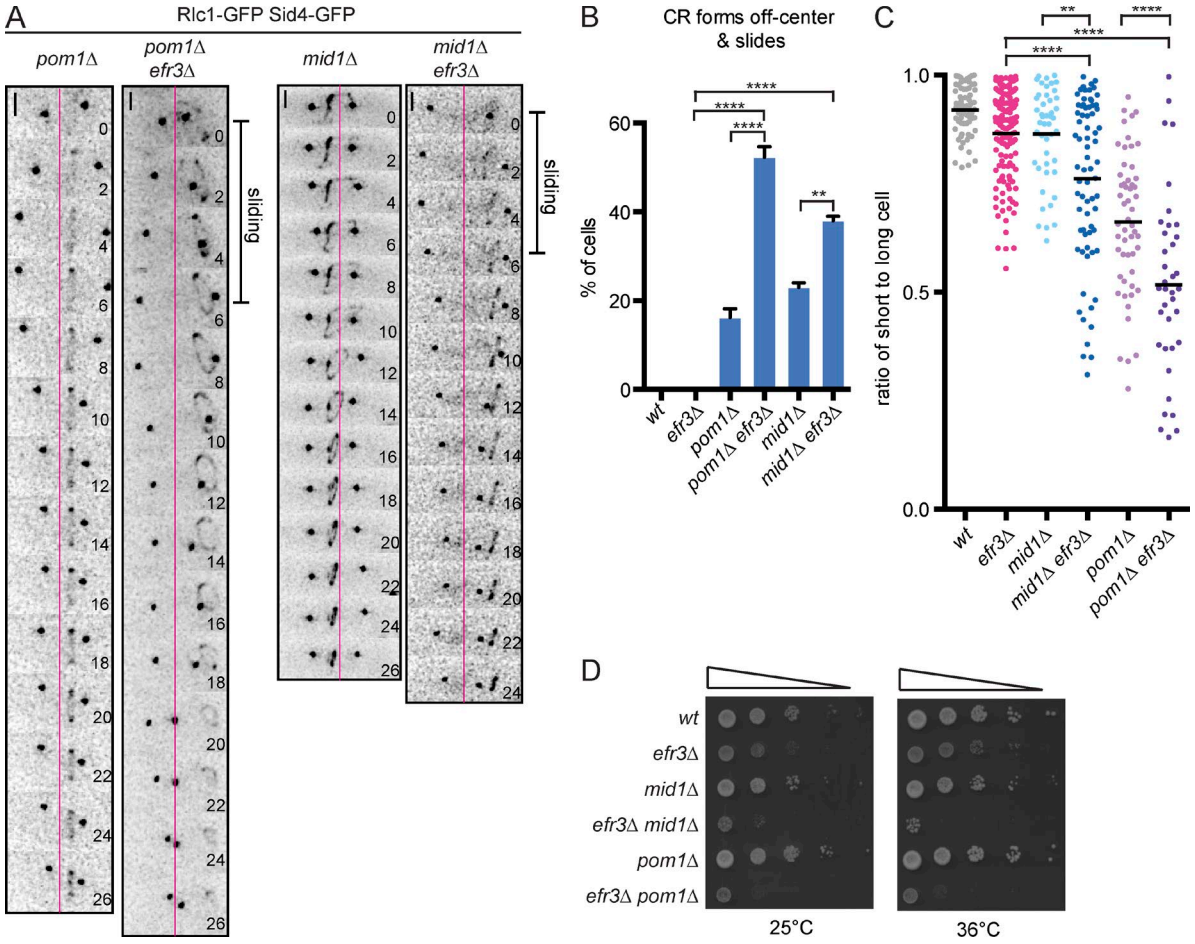

Figure 4. **The Stt4 complex and CR positioning machinery cooperate in septum positioning.** (A) Live-cell imaging of indicated strains expressing Rlc1-GFP and Sid4-GFP. Magenta lines mark the cell center. Bars, 2 µm. (B) Quantification of the frequency of events shown in A where the CR forms off center and slides. Error bars represent SEM. **, P ≤ 0.01; ****, P ≤ 0.0001; one-way ANOVA. (C) Quantification of CR sliding. Individual points represent the ratio of the length of short to long cells at septation, and black bars denote means. (D) Growth assay of serial 10-fold dilutions of the indicated strains at the indicated temperatures.

MSD analysis

Time-lapse images of a medial z slice of a strain expressing a CR and spindle pole body marker were acquired every 10 s, registered for both differential interference contrast and fluorescent channels using the ImageJ plugin Image Stabilizer (Li, 2008), and then merged together to determine the position of the ring relative to the cell boundary. Cytokinetic ring positions were recorded for 17 WT and 18 *efr3Δ* mutant cells, beginning when the CR was fully formed. Individual trajectories were obtained by reslicing the time-lapse images to a 3-pixel-wide line along the cell boundary and tracking the position of the ring with subpixel resolution using the ImageJ plugin TrackMate (Tinevez et al., 2017). Total absolute displacements for WT trajectories over a 300-s period were measured to be 83 ± 66 nm (standard deviation; $n = 34$ tracks from 17 cells), which is within the spatial resolution of the imaging (pixel size, 106 nm). For *efr3Δ* mutant cells, one-dimensional position over time data were used to perform MSD analysis for the first 300 s of the data using MATLAB (R2016b; MathWorks) and the msdanalyzer tool as previously described (Tarantino et al., 2014). MSD data for *efr3Δ* mutant cells were fit by the second-degree polynomial function:

$$MSD(\tau) = 2D\tau + v^2\tau^2 + \sigma$$

where D is the diffusion coefficient, v is the drift velocity, and σ is the noise term. The fitting procedure yielded:

$$MSD(\tau) = \left(7.42 \times 10^{-5}\ \frac{\mu m^2}{s}\right)\tau + \left(1.82 \times 10^{-6}\ \frac{\mu m^2}{s^2}\right)\tau^2 + \left(1.24 \times 10^{-3}\ \mu m^2\right)$$

$r^2 = 99.90\%$.

Protein methods and mass spectrometry

Cell pellets were snap frozen in dry ice–ethanol baths. Lysates were prepared using a Fastprep cell homogenizer (MP Biomedicals). Immunoprecipitations were performed as previously described (Gould et al., 1991) in NP-40 buffer for native lysates. Protein samples were resolved by SDS-PAGE and transferred to PVDF membrane (Immobilon P; EMD Millipore). Anti-HA (12CA5), anti-Flag (M2; Sigma-Aldrich), anti-GFP (Roche), anti-Cdc15 serum (Roberts-Galbraith et al., 2009), or anti-PSTAIRE (Cdc2; Sigma-Aldrich) were used in immunoprecipitations and/or as primary antibodies in immunoblotting. Secondary antibodies were conjugated to IRDye680LT or IRDye800 (LI-COR Biosciences). Blotted proteins were detected via Odyssey (LI-COR Biosciences).

Purification of Efr3-TAP and subsequent identification of interacting proteins by mass spectrometry were performed as previously described (Gould et al., 2004; Chen et al., 2013; Elmore et al., 2014) with the following changes: a newer version of Scaffold (Scaffold v4.4.1.1;

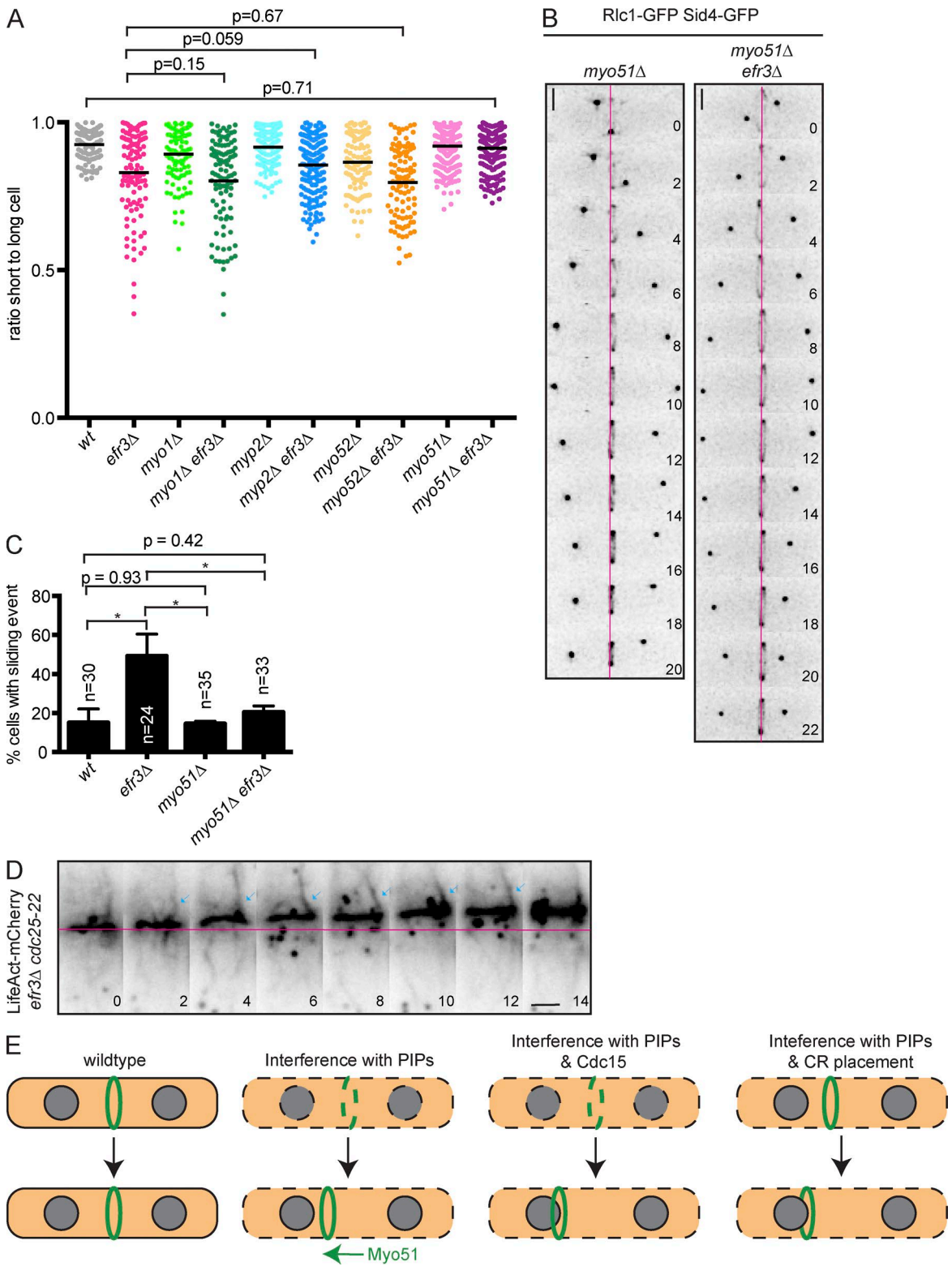

Figure 5. ***efr3Δ* CR sliding events depend on Myo51.** (A) Quantification of off-center septa in the indicated strains. Individual points represent the ratio of the length of short to long daughter cells at septation, and black bars denote means. (B) Live-cell imaging of indicated strains expressing Rlc1-GFP and Sid4-GFP at 2-min intervals. Magenta lines mark the cell center. (C) Quantification of the frequency of CR sliding events in the indicated strains. Error bars represent SEM. *, $P \leq 0.05$; one-way ANOVA. (D) Montage of 2-min-interval time-lapse imaging of *LifeAct-mCherry* in *efr3Δ cdc25-22*. Montage is of a single z slice, and blue arrows indicate an actin cable in close proximity to a sliding CR. Bars, 2 µm. (E) Model for CR anchoring in cytokinesis. Proper PIP composition, dependent on Efr3, promotes CR anchoring. When PM lipid and CR protein composition is altered, CRs can slide. Cdc15 is an independent mechanism for CR anchoring as *cdc15* mutants combined with *efr3Δ* results in exacerbated CR sliding defects. Disruption of CR positioning machinery in combination with *efr3Δ* leads to exacerbation of off-center septa.

Proteome Software) was used, and the minimum peptide identification probability was changed to 95.0%.

All ANOVA statistical analyses used Tukey's post hoc analysis.

Online supplemental material

Fig. S1 shows that Efr3 and Ypp1 coimmunoprecipitated, that Ypp1 and Stt4 were purified from an *efr3*-TAP, and that *stt4* and *ypp1* are essential genes. Fig. S2 shows that *efr3Δ* does not have altered CR kinetics, that *pos5Δ* does not have off-center septa, and that *efr3Δ pxl1Δ* is synthetically lethal. Fig. S3 shows *efr3Δ* and *myo2-E1* are synthetically lethal, that *efr3Δ* off-center septa do not depend on Myo2, that *cdc15–core 4A* and *pxl1Δ* CR sliding do not depend on a myosin, that the N and C termini of Myo51 are necessary for CR sliding in *efr3Δ*, and MSD analysis of *efr3Δ* sliding CRs. Table S1 includes *S. pombe* strains used in this study, and Table S2 contains the mass spectrometry results identified in an Efr3-TAP pulldown.

Acknowledgments

We thank Drs. J. Beckley, N. McDonald, and S. Cullati for critical reading of this manuscript and Dr. J.-Q. Wu for strains.

We are grateful for the following support: National Institutes of Health grants GM101035 (to K.L. Gould), GM119552 (to M. Zanic), and T32GM008554-21 (to C.E. Snider) as well as American Heart Association grant 14PRE19740000 (to A.H. Willet). M. Zanic acknowledges the support from the Human Frontier Science Program and the Searle Scholars Program.

The authors declare no competing financial interests.

Author contributions: C.E. Snider, A.H. Willet, M. Zanic, and K.L. Gould were responsible for the experimental design. C.E. Snider, A.H. Willet, J.-S. Chen, and G. Arpağ performed all of the experiments. C.E. Snider, A.H. Willet, and K.L. Gould wrote the manuscript with contributions from J.-S. Chen, G. Arpağ, and M. Zanic.

Submitted: 11 May 2017
Revised: 23 June 2017
Accepted: 7 July 2017

References

Arai, R., and I. Mabuchi. 2002. F-actin ring formation and the role of F-actin cables in the fission yeast S*chizosaccharomyces pombe. J. Cell Sci.* 115:887–898.

Arasada, R., and T.D. Pollard. 2014. Contractile ring stability in *S. pombe* depends on F-BAR protein Cdc15p and Bgs1p transport from the Golgi complex. *Cell Reports.* 8:1533–1544. http://dx.doi.org/10.1016/j.celrep.2014.07.048

Atilgan, E., V. Magidson, A. Khodjakov, and F. Chang. 2015. Morphogenesis of the fission yeast cell through cell wall expansion. *Curr. Biol.* 25:2150–2157. http://dx.doi.org/10.1016/j.cub.2015.06.059

Audhya, A., and S.D. Emr. 2002. Stt4 PI 4-kinase localizes to the plasma membrane and functions in the Pkc1-mediated MAP kinase cascade. *Dev. Cell.* 2:593–605. http://dx.doi.org/10.1016/S1534-5807(02)00168-5

Bähler, J., and J.R. Pringle. 1998. Pom1p, a fission yeast protein kinase that provides positional information for both polarized growth and cytokinesis. *Genes Dev.* 12:1356–1370. http://dx.doi.org/10.1101/gad.12.9.1356

Bähler, J., A.B. Steever, S. Wheatley, Y. Wang, J.R. Pringle, K.L. Gould, and D. McCollum. 1998a. Role of polo kinase and Mid1p in determining the site of cell division in fission yeast. *J. Cell Biol.* 143:1603–1616. http://dx.doi.org/10.1083/jcb.143.6.1603

Bähler, J., J.Q. Wu, M.S. Longtine, N.G. Shah, A. McKenzie III, A.B. Steever, A. Wach, P. Philippsen, and J.R. Pringle. 1998b. Heterologous modules for efficient and versatile PCR-based gene targeting in *Schizosaccharomyces pombe*. *Yeast.* 14:943–951. http://dx.doi.org/10.1002/(SICI)1097-0061(199807)14:10<943::AID-YEA292>3.0.CO;2-Y

Baird, D., C. Stefan, A. Audhya, S. Weys, and S.D. Emr. 2008. Assembly of the PtdIns 4-kinase Stt4 complex at the plasma membrane requires Ypp1 and Efr3. *J. Cell Biol.* 183:1061–1074. http://dx.doi.org/10.1083/jcb.200804003

Balasubramanian, M.K., D. McCollum, L. Chang, K.C.Y. Wong, N.I. Naqvi, X. He, S. Sazer, and K.L. Gould. 1998. Isolation and characterization of new fission yeast cytokinesis mutants. *Genetics.* 149:1265–1275.

Basi, G., E. Schmid, and K. Maundrell. 1993. TATA box mutations in the Schizosaccharomyces pombe nmt1 promoter affect transcription efficiency but not the transcription start point or thiamine repressibility. *Gene*. 123:131–136. http://dx.doi.org/10.1016/0378-1119(93)90552-E8422997

Bohnert, K.A., and K.L. Gould. 2011. On the cutting edge: post-translational modifications in cytokinesis. *Trends Cell Biol.* 21:283–292. http://dx.doi.org/10.1016/j.tcb.2011.01.006

Brill, J.A., G.R. Hime, M. Scharer-Schuksz, and M.T. Fuller. 2000. A phospholipid kinase regulates actin organization and intercellular bridge formation during germline cytokinesis. *Development.* 127:3855–3864.

Cauvin, C., and A. Echard. 2015. Phosphoinositides: Lipids with informative heads and mastermind functions in cell division. *Biochim. Biophys. Acta.* 1851:832–843. http://dx.doi.org/10.1016/j.bbalip.2014.10.013

Celton-Morizur, S., N. Bordes, V. Fraisier, P.T. Tran, and A. Paoletti. 2004. C-terminal anchoring of mid1p to membranes stabilizes cytokinetic ring position in early mitosis in fission yeast. *Mol. Cell. Biol.* 24:10621–10635. http://dx.doi.org/10.1128/MCB.24.24.10621-10635.2004

Chang, F., A. Woollard, and P. Nurse. 1996. Isolation and characterization of fission yeast mutants defective in the assembly and placement of the contractile actin ring. *J. Cell Sci.* 109:131–142.

Cheffings, T.H., N.J. Burroughs, and M.K. Balasubramanian. 2016. Actomyosin ring formation and tension generation in eukaryotic cytokinesis. *Curr. Biol.* 26:R719–R737. http://dx.doi.org/10.1016/j.cub.2016.06.071

Chen, J.-S., M.R. Broadus, J.R. McLean, A. Feoktistova, L. Ren, and K.L. Gould. 2013. Comprehensive proteomics analysis reveals new substrates and regulators of the fission yeast clp1/cdc14 phosphatase. *Mol. Cell. Proteomics.* 12:1074–1086. http://dx.doi.org/10.1074/mcp.M112.025924

Chen, J.-S., J.R. Beckley, N.A. McDonald, L. Ren, M. Mangione, S.J. Jang, Z.C. Elmore, N. Rachfall, A. Feoktistova, C.M. Jones, et al. 2015. Identification of new players in cell division, DNA damage response, and morphogenesis through construction of *Schizosaccharomyces pombe* deletion strains. *Genes Genomes Genetics.* 5:361–370. http://dx.doi.org/10.1534/g3.114.015701

Cortés, J.C.G., N. Pujol, M. Sato, M. Pinar, M. Ramos, B. Moreno, M. Osumi, J.C. Ribas, and P. Pérez. 2015. Cooperation between paxillin-like protein Pxl1 and glucan synthase Bgs1 is essential for actomyosin ring stability and septum formation in fission yeast. *PLoS Genet.* 11:e1005358. http://dx.doi.org/10.1371/journal.pgen.1005358

D'Avino, P.P. 2009. How to scaffold the contractile ring for a safe cytokinesis – lessons from Anillin-related proteins. *J. Cell Sci.* 122:1071–1079. http://dx.doi.org/10.1242/jcs.034785

Davidson, R., J.A. Pontasch, and J.-Q. Wu. 2016. Sbg1 is a novel regulator for the localization of the β-glucan synthase Bgs1 in fission yeast. *PLoS One.* 11:e0167043. http://dx.doi.org/10.1371/journal.pone.0167043

Eggert, U.S., A.A. Kiger, C. Richter, Z.E. Perlman, N. Perrimon, T.J. Mitchison, and C.M. Field. 2004. Parallel chemical genetic and genome-wide RNAi screens identify cytokinesis inhibitors and targets. *PLoS Biol.* 2:e379. http://dx.doi.org/10.1371/journal.pbio.0020379

Elmore, Z.C., J.R. Beckley, J.-S. Chen, and K.L. Gould. 2014. Histone H2B ubiquitination promotes the function of the anaphase-promoting complex/cyclosome in *Schizosaccharomyces pombe*. *Genes Genomes Genetics.* 4:1529–1538. http://dx.doi.org/10.1534/g3.114.012625

Emoto, K., H. Inadome, Y. Kanaho, S. Narumiya, and M. Umeda. 2005. Local change in phospholipid composition at the cleavage furrow is essential for completion of cytokinesis. *J. Biol. Chem.* 280:37901–37907. http://dx.doi.org/10.1074/jbc.M504282200

Field, S.J., N. Madson, M.L. Kerr, K.A.A. Galbraith, C.E. Kennedy, M. Tahiliani, A. Wilkins, and L.C. Cantley. 2005. PtdIns(4,5)P2 functions at the cleavage furrow during cytokinesis. *Curr. Biol.* 15:1407–1412. http://dx.doi.org/10.1016/j.cub.2005.06.059

Ge, W., and M.K. Balasubramanian. 2008. Pxl1p, a paxillin-related protein, stabilizes the actomyosin ring during cytokinesis in fission yeast. *Mol. Biol. Cell.* 19:1680–1692. http://dx.doi.org/10.1091/mbc.E07-07-0715

Gould, G.W. 2016. Animal cell cytokinesis: the role of dynamic changes in the plasma membrane proteome and lipidome. *Semin. Cell Dev. Biol.* 53:64–73. http://dx.doi.org/10.1016/j.semcdb.2015.12.012

Gould, K.L., S. Moreno, D.J. Owen, S. Sazer, and P. Nurse. 1991. Phosphorylation at Thr167 is required for Schizosaccharomyces pombe p34cdc2 function. *EMBO J.* 10:3297–3309.

Gould, K.L., L. Ren, A.S. Feoktistova, J.L. Jennings, and A.J. Link. 2004. Tandem affinity purification and identification of protein complex

components. *Methods.* 33:239–244. http://dx.doi.org/10.1016/j.ymeth.2003.11.019

Goyal, A., M. Takaine, V. Simanis, and K. Nakano. 2011. Dividing the spoils of growth and the cell cycle: The fission yeast as a model for the study of cytokinesis. *Cytoskeleton (Hoboken).* 68:69–88. http://dx.doi.org/10.1002/cm.20500

Hachet, O., and V. Simanis. 2008. Mid1p/anillin and the septation initiation network orchestrate contractile ring assembly for cytokinesis. *Genes Dev.* 22:3205–3216. http://dx.doi.org/10.1101/gad.1697208

Hachet, O., M. Berthelot-Grosjean, K. Kokkoris, V. Vincenzetti, J. Moosbrugger, and S.G. Martin. 2011. A phosphorylation cycle shapes gradients of the DYRK family kinase Pom1 at the plasma membrane. *Cell.* 145:1116–1128. http://dx.doi.org/10.1016/j.cell.2011.05.014

Hayles, J., V. Wood, L. Jeffery, K.-L. Hoe, D.-U. Kim, H.-O. Park, S. Salas-Pino, C. Heichinger, and P. Nurse. 2013. A genome-wide resource of cell cycle and cell shape genes of fission yeast. *Open Biol.* 3:130053. http://dx.doi.org/10.1098/rsob.130053

Huang, J., Y. Huang, H. Yu, D. Subramanian, A. Padmanabhan, R. Thadani, Y. Tao, X. Tang, R. Wedlich-Soldner, and M.K. Balasubramanian. 2012. Nonmedially assembled F-actin cables incorporate into the actomyosin ring in fission yeast. *J. Cell Biol.* 199:831–847. http://dx.doi.org/10.1083/jcb.201209044

Huang, Y., H. Yan, and M.K. Balasubramanian. 2008. Assembly of normal actomyosin rings in the absence of Mid1p and cortical nodes in fission yeast. *J. Cell Biol.* 183:979–988. http://dx.doi.org/10.1083/jcb.200806151

Kechad, A., S. Jananji, Y. Ruella, and G.R.X. Hickson. 2012. Anillin acts as a bifunctional linker coordinating midbody ring biogenesis during cytokinesis. *Curr. Biol.* 22:197–203. http://dx.doi.org/10.1016/j.cub.2011.11.062

Keeney, J.B., and J.D. Boeke. 1994. Efficient targeted integration at leu1-32 and ura4-294 in *Schizosaccharomyces pombe. Genetics.* 136:849–856.

Kitayama, C., A. Sugimoto, and M. Yamamoto. 1997. Type II myosin heavy chain encoded by the m*yo2* gene composes the contractile ring during cytokinesis in S*chizosaccharomyces pombe. J. Cell Biol.* 137:1309–1319. http://dx.doi.org/10.1083/jcb.137.6.1309

Laporte, D., V.C. Coffman, I.J. Lee, and J.Q. Wu. 2011. Assembly and architecture of precursor nodes during fission yeast cytokinesis. *J. Cell Biol.* 192:1005–1021. http://dx.doi.org/10.1083/jcb.201008171

Lee, I.-J., V.C. Coffman, and J.-Q. Wu. 2012. Contractile-ring assembly in fission yeast cytokinesis: Recent advances and new perspectives. *Cytoskeleton (Hoboken).* 69:751–763. http://dx.doi.org/10.1002/cm.21052

Li, K. 2008. The image stabilizer plugin for ImageJ.http://www.cs.cmu.edu/~kangli/code/image_stabilizer.html

Ling, Y., C.J. Stefan, J.A. Macgurn, A. Audhya, and S.D. Emr. 2012. The dual PH domain protein Opy1 functions as a sensor and modulator of PtdIns(4,5)P_2 synthesis. *EMBO J.* 31:2882–2894. http://dx.doi.org/10.1038/emboj.2012.127

Marks, J., and J.S. Hyams. 1985. Localization of F-actin through the cell division cycle of S*chizosaccharomyces pombe. Eur. J. Cell Biol.* 39:27–32.

Marks, J., I.M. Hagan, and J.S. Hyams. 1986. Growth polarity and cytokinesis in fission yeast: The role of the cytoskeleton. *J. Cell Sci. Suppl.* 5:229–241. http://dx.doi.org/10.1242/jcs.1986.Supplement_5.15

McDonald, N.A., C.W. Vander Kooi, M.D. Ohi, and K.L. Gould. 2015. Oligomerization but not membrane bending underlies the function of certain F-BAR proteins in cell motility and cytokinesis. *Dev. Cell.* 35:725–736. http://dx.doi.org/10.1016/j.devcel.2015.11.023

Meddins, A.K., P. Nurse, and K.L. Gould. 1993. Analysis of 5′ flanking sequences from the Schizosaccharomyces pombe cdc2 gene. *Gene*. 127:145–148. http://dx.doi.org/10.1016/0378-1119(93)90630-L8486281

Mishra, M., Y. Huang, P. Srivastava, R. Srinivasan, M. Sevugan, R. Shlomovitz, N. Gov, M. Rao, and M. Balasubramanian. 2012. Cylindrical cellular geometry ensures fidelity of division site placement in fission yeast. *J. Cell Sci.* 125:3850–3857. http://dx.doi.org/10.1242/jcs.103788

Mishra, M., J. Kashiwazaki, T. Takagi, R. Srinivasan, Y. Huang, M.K. Balasubramanian, and I. Mabuchi. 2013. In vitro contraction of cytokinetic ring depends on myosin II but not on actin dynamics. *Nat. Cell Biol.* 15:853–859. http://dx.doi.org/10.1038/ncb2781

Muñoz, J., J.C. Cortés, M. Sipiczki, M. Ramos, J.A. Clemente-Ramos, M.B. Moreno, I.M. Martins, P. Pérez, and J.C. Ribas. 2013. Extracellular cell wall β(1,3)glucan is required to couple septation to actomyosin ring contraction. *J. Cell Biol.* 203:265–282. http://dx.doi.org/10.1083/jcb.201304132

Nakatsu, F., J.M. Baskin, J. Chung, L.B. Tanner, G. Shui, S.Y. Lee, M. Pirruccello, M. Hao, N.T. Ingolia, M.R. Wenk, and P. De Camilli. 2012. PtdIns4P synthesis by PI4KIIIα at the plasma membrane and its impact on plasma membrane identity. *J. Cell Biol.* 199:1003–1016. http://dx.doi.org/10.1083/jcb.201206095

Pardo, M., and P. Nurse. 2003. Equatorial retention of the contractile actin ring by microtubules during cytokinesis. *Science.* 300:1569–1574. http://dx.doi.org/10.1126/science.1084671

Piekny, A.J., and M. Glotzer. 2008. Anillin is a scaffold protein that links RhoA, actin, and myosin during cytokinesis. *Curr. Biol.* 18:30–36. http://dx.doi.org/10.1016/j.cub.2007.11.068

Pollard, T.D., and J.-Q. Wu. 2010. Understanding cytokinesis: lessons from fission yeast. *Nat. Rev. Mol. Cell Biol.* 11:149–155. http://dx.doi.org/10.1038/nrm2834

Proctor, S.A., N. Minc, A. Boudaoud, and F. Chang. 2012. Contributions of turgor pressure, the contractile ring, and septum assembly to forces in cytokinesis in fission yeast. *Curr. Biol.* 22:1601–1608. http://dx.doi.org/10.1016/j.cub.2012.06.042

Rincon, S.A., and A. Paoletti. 2016. Molecular control of fission yeast cytokinesis. *Semin. Cell Dev. Biol.* 53:28–38. http://dx.doi.org/10.1016/j.semcdb.2016.01.007

Roberts-Galbraith, R.H., J.-S. Chen, J. Wang, and K.L. Gould. 2009. The SH3 domains of two PCH family members cooperate in assembly of the *Schizosaccharomyces pombe* contractile ring. *J. Cell Biol.* 184:113–127. http://dx.doi.org/10.1083/jcb.200806044

Sethi, K., S. Palani, J.C. Cortés, M. Sato, M. Sevugan, M. Ramos, S. Vijaykumar, M. Osumi, N.I. Naqvi, J.C. Ribas, and M. Balasubramanian. 2016. A new membrane protein Sbg1 links the contractile ring apparatus and septum synthesis machinery in fission yeast. *PLoS Genet.* 12:e1006383. http://dx.doi.org/10.1371/journal.pgen.1006383

Sohrmann, M., C. Fankhauser, C. Brodbeck, and V. Simanis. 1996. The dmf1/mid1 gene is essential for correct positioning of the division septum in fission yeast. *Genes Dev.* 10:2707–2719. http://dx.doi.org/10.1101/gad.10.21.2707

Stefan, C.J., A. Audhya, and S.D. Emr. 2002. The yeast synaptojanin-like proteins control the cellular distribution of phosphatidylinositol (4,5)-bisphosphate. *Mol. Biol. Cell.* 13:542–557. http://dx.doi.org/10.1091/mbc.01-10-0476

Sun, L., R. Guan, I.J. Lee, Y. Liu, M. Chen, J. Wang, J.-Q. Wu, and Z. Chen. 2015. Mechanistic insights into the anchorage of the contractile ring by anillin and Mid1. *Dev. Cell.* 33:413–426. http://dx.doi.org/10.1016/j.devcel.2015.03.003

Tarantino, N., J.Y. Tinevez, E.F. Crowell, B. Boisson, R. Henriques, M. Mhlanga, F. Agou, A. Israël, and E. Laplantine. 2014. TNF and IL-1 exhibit distinct ubiquitin requirements for inducing NEMO-IKK supramolecular structures. *J. Cell Biol.* 204:231–245. http://dx.doi.org/10.1083/jcb.201307172

Tinevez, J.-Y., N. Perry, J. Schindelin, G.M. Hoopes, G.D. Reynolds, E. Laplantine, S.Y. Bednarek, S.L. Shorte, and K.W. Eliceiri. 2017. TrackMate: An open and extensible platform for single-particle tracking. *Methods.* 115:80–90. http://dx.doi.org/10.1016/j.ymeth.2016.09.016

Wach, A., A. Brachat, R. Pöhlmann, and P. Philippsen. 1994. New heterologous modules for classical or PCR-based gene disruptions in *Saccharomyces cerevisiae*. *Yeast.* 10:1793–1808. http://dx.doi.org/10.1002/yea.320101310

Wachtler, V., Y. Huang, J. Karagiannis, and M.K. Balasubramanian. 2006. Cell cycle-dependent roles for the FCH-domain protein Cdc15p in formation of the actomyosin ring in *Schizosaccharomyces pombe*. *Mol. Biol. Cell.* 17:3254–3266. http://dx.doi.org/10.1091/mbc.E05-11-1086

Wang, N., L. Lo Presti, Y.H. Zhu, M. Kang, Z. Wu, S.G. Martin, and J.-Q. Wu. 2014. The novel proteins Rng8 and Rng9 regulate the myosin-V Myo51 during fission yeast cytokinesis. *J. Cell Biol.* 205:357–375. http://dx.doi.org/10.1083/jcb.201308146

Waters, J.C. 2009. Accuracy and precision in quantitative fluorescence microscopy. *J. Cell Biol.* 185:1135–1148. http://dx.doi.org/10.1083/jcb.200903097

Werler, P.J.H., E. Hartsuiker, and A.M. Carr. 2003. A simple Cre-*loxP* method for chromosomal N-terminal tagging of essential and non-essential *Schizosaccharomyces pombe* genes. *Gene.* 304:133–141. http://dx.doi.org/10.1016/S0378-1119(03)00402-5

Willet, A.H., N.A. McDonald, and K.L. Gould. 2015. Regulation of contractile ring formation and septation in *Schizosaccharomyces pombe*. *Curr. Opin. Microbiol.* 28:46–52. http://dx.doi.org/10.1016/j.mib.2015.08.001